ORIGINAL RESEARCH

# Synthesizing green carbon dots with exceptionally high yield from biomass hydrothermal carbon

Yushuang Zhao · Shuangshuang Jing · Xinwen Peng · Zehong Chen · Yijie Hu · Hao Zhuo · Runcang Sun · Linxin Zhong

**Abstract** Carbon dots (CDs), with high photostability, tunable excitation and emission wavelength, excellent biocompatibility, and environmental friendliness, attract great interest because of their promising applications in various fields. The synthesis of CDs from renewable biomass is especially attractive due to its sustainable and cost-efficient feature. However, one of the major problems for this route is the low yield of CDs. To overcome this issue, we propose a facile, universal, and highly effective synthesis method to prepare fluorescent CDs from various biomass hydrothermal carbons (HTCs). As compared with the current methods for synthesizing biomass derived CDs, our approach offers ultrahigh yield (42.5% based on the weight of biomass and 99.0% based on the weight of HTC) that is much higher than those obtained from other methods. The physiochemical properties of the as-prepared CDs can be tuned by reaction temperature. Furthermore, the PL quantum yield is high up to 16.6%, and is correlated with the surface chemical groups and conjugated π-domains of the carbon core in CDs. The fluorescence of CDs is effectively and selectively quenched by $Cu^{2+}$, which enables CDs applying as fluorescent $Cu^{2+}$ nanoprobe with a linear range of 0–30 μmol $L^{-1}$ and a detection limit of 85 nmol $L^{-1}$. Due to simple operation, mild condition, and low cost of the process, this method have a great potential in the large-scale synthesis and application of CDs from biomass.

Yushuang Zhao and Shuangshuang Jing have contributed equally to this paper.

**Electronic supplementary material** The online version of this article (https://doi.org/10.1007/s10570-019-02807-0) contains supplementary material, which is available to authorized users.

Y. Zhao · S. Jing · X. Peng · Z. Chen ·
Y. Hu · H. Zhuo · L. Zhong (✉)
State Key Laboratory of Pulp and Paper Engineering,
South China University of Technology, Guangzhou,
People's Republic of China
e-mail: lxzhong0611@scut.edu.cn

R. Sun
Center for Lignocellulose Science and Engineering, and
Liaoning Key Laboratory Pulp and Paper Engineering,
Dalian Polytechnic University, Dalian, People's Republic
of China

## Graphic abstract
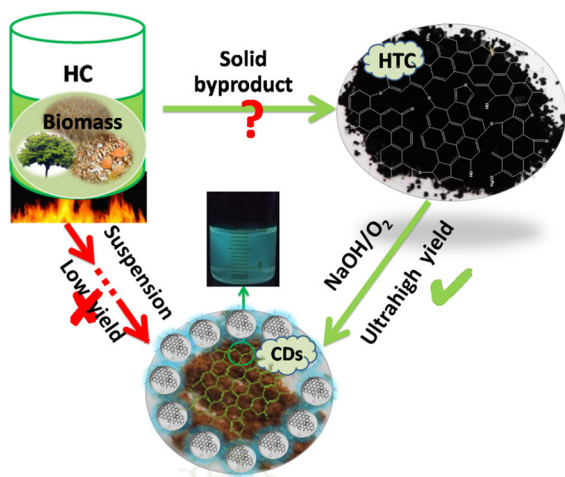


**Keywords** Biomass · Lignocellulose · Hydrothermal carbon · Green carbon dots · Hydrothermal

## Introduction

Carbon dots (CDs), the quasi-spherical nanoparticles with size less than 10 nm, are a novel class of nano carbons. Owing to their excellent biological properties and photochemical performances, rich photoluminescence (PL), and tunable surface chemistry, CDs attract great interest in bioimaging, biosensing, optronics, catalysis, and energy devices (solar cells, batteries and super-capacitors) (Li et al. 2013a; Ran et al. 2013; Yuan et al. 2017; Zhu et al. 2013). CDs are classified into several categories, namely, tiny sized carbon nanoparticles, graphene quantum dots, graphitic carbon quantum dots, amorphous carbon dots, and polymer dots (Gao et al. 2017). Correspondingly, the synthetic methods for CDs are generally divided into top-down and bottom-up approaches. Top-down method including laser ablation (Hu et al. 2009), acid hydrolysis (Ye et al. 2013), discharge (Bao et al. 2011), and electrochemical oxidation (Zhao et al. 2008), usually produces CDs from bulk carbon materials, such as graphite, CNTs, and carbon black. However, this method generally requires expensive equipment and materials, as well as harsh conditions. Bottom-up method, synthesizing CDs from abundant

and low-cost organic molecules, involves hydrothermal (Zhu et al. 2013), microwave pyrolysis (Jaiswal et al. 2012; Yuan et al. 2018), and solvothermal (Yuan et al. 2017), exhibiting low cost, eco-friendliness, and easy chemical modification.

Hydrothermal synthesis is widely adopted due to the green process, easy operation, and mild reaction conditions (Li et al. 2013b; Wang et al. 2014a; Wang and Hu 2014). The properties of prepared CDs mainly depend on the types of precursors such as small molecules, synthetic polymers, and biomass (He et al. 2011; Li et al. 2015; Liu et al. 2018a, b; Xiong et al. 2017). Up to now, great efforts have been made to develop green CDs through hydrothermally treating various biomass resources containing paper ash (Wei et al. 2013), willow bark (Qin et al. 2013), wheat straw (Yuan et al. 2015), grass (Liu et al. 2012), protein (Wu et al. 2013; Zhang et al. 2012b), chitosan (Wang et al. 2016a), fiber (Yang et al. 2016), and lignin (Chen et al. 2016). However, the production yields are low. For example, Chen et al. (2016) prepared lignin-derived CDs with low yield of 0.8–12.06 wt% through hydrothermal treatment. Yang et al. (2012) synthesized fluorescent carbon nanoparticles by hydrothermally carbonizing chitosan with a low yield of 7.8%. In fact, most of biomass is converted into solid carbon product (hydrothermal carbon) during hydrothermal process, instead of CDs in the suspension.

In this paper, a universal, low-cost, and high-efficiency route was developed for high-yield synthesis of fluorescent CDs from HTC, which is completely different from the traditional method to obtain CDs from hydrothermal suspension. It is found that HTC can be transferred into CDs by low-concentration sodium hydroxide solution and oxygen treatment. The yields of CDs are extremely high (67–99%), which is much higher than those of CDs from the hydrothermal suspension. The as-prepared CDs show excellent photoluminescence properties with high quantum yield (QY), excitation-dependent PL behaviour, up-conversion properties, and long-term photostability. Furthermore, the CDs are used as a fluorescent sensing material for selective detection of $Cu^{2+}$. This new synthetic method is also highly effective for various biomass resources including hemicelluloses, lignin, cellulose, and chitosan, and thus opens up new way for the operable and highly value-added application of HTC and the industrial synthesis and application of CDs.

## Materials and methods

### Materials

Hemicelluloses, lignin, chitosan, and α-cellulose were purchased from Aladdin (China). Sodium hydroxide (ACS, 97%) and hydrochloric acid (36–38%) were from Guangzhou Chemical Reagent (China). $FeCl_3$, $FeCl_2$, KCl, $MgCl_2$, $CuCl_2$, $CoCl_2$, $BaCl_2$, $ZnCl_2$, $NiCl_2$, $CrCl_3$, $AlCl_3$, and $CaCl_2$ were purchased from Tianjin Damao Chemical Reagent (China). Quinine sulfate dehydrate (AR, 99.0%, Biotech) was purchased from Aladdin (China). All the reagents were of analytical grade and used directly without any further purification.

### Preparation of hydrothermal carbon (HTC)

In a typical preparation, 1.5 g biomass (hemicelluloses, lignin, chitosan, and cellulose) was dispersed in ultrapure water (30 mL) by stirring. The mixture was transferred to stainless steel autoclaves (SLM-50). Then the chamber was put into a furnace after sealing. The hydrothermal reaction was carried out in the furnace under 600 rpm at 240 °C for 6 h. After cooling to room temperature, the hydrothermal carbon was collected by vacuum filtering with a 0.22 μm microporous membrane and thoroughly washed with deionized water, and then dried in a vacuum oven at 80 °C overnight.

### Synthesis of CDs

50 mg of the resultant hydrothermal carbon was added into 50 mL Teflon-lined stainless-steel autoclave (SLM-50) with 25 mL of 0.1 M NaOH. The chamber was sealed, and then $O_2$ was blown into the autoclave to remove air and keep the pressure at 1 MPa. After that, the autoclave was heated at 160 °C (or 100 °C, 120 °C, 140 °C, and 180 °C) for 1 h with stirring (1000 rpm). After being naturally cooled to room temperature, the obtained yellow solution containing water-dispersion CDs was neutralized by HCl and filtered through a 0.22 μm microporous membrane. Then, the filtrate was dialyzed in a dialysis bag (retaining molecular weight: 500 Da) in deionized water for 5 days. Finally, the solution was freeze-dried to obtain the purified CDs for characterization and property measurements. Samples denoted as $CDs_{100}$, $CDs_{120}$, $CDs_{140}$, $CDs_{160}$ and $CDs_{180}$ were synthesized at 100 °C, 120 °C, 140 °C, 160 °C and 180 °C, respectively.

### Characterization

Transmission electron microscopy (TEM) and the high-resolution transmission electron microscopy (HR-TEM) images were obtained using a JEM-2100F at 200 kV. Samples for TEM measurements were prepared by placing a drop of the colloidal solution of CDs on a carbon-coated copper grid and then dried at room temperature. The morphologies of the HTCs were observed using scanning electron microscopy (SEM, ZEISS Merlin, Germany). X-ray diffraction (XRD) patterns were monitored by a Bruker D8 diffractometer using Cu Kα radiation ($\lambda = 0.15418$ nm) as an X-ray source. Raman spectra were recorded by a Raman spectrometer (LabRAM ARAMIS – Horiba Jobin–Yvon, France) operating with 532 nm laser. X-ray photoelectron spectra (XPS) were recorded by X-ray Photoelectron Spectrometer (K-Alpha$^+$, Thermo fisher Scientific) with an exciting source of Al·Kα (1486.6 eV, 6 mA × 12 kV). The FT-IR spectra were recorded by a FT-IR spectrophotometer (TENSOR27, Germany). The tested sample was obtained by mixing CDs and KBr power and pressing. Elemental analysis was carried out by using a Vario EL cube instrument (Elementar, Geman), and C and H contents were tested. Solid-state cross polarization/magic angle spinning (CP MAS) $^{13}$C NMR experiments was performed on a Bruker Avance III 400 MHz (9.4 T) spectrometer with a 4 mm zirconia rotor as sample holder spinning at MAS rate of 5 kHz. The chemical shift reference for $^{13}$C was tetramethylsilane at 0 ppm. UV–visible absorption spectra of CDs were recorded by using a South Korea S3100 UV–Vis spectrophotometer. Fluorescence spectra were recorded by the HORIBA Scientific FluoroMax-4 fluorescence spectrophotometer.

### Fluorescence QY measurement

Quantum yield was measured according to the established procedure by using quinine sulfate in 0.10 M $H_2SO_4$ solution as a reference. The quinine sulfate (QR = 0.54) dissolved in 0.1 M $H_2SO_4$ (refractive index $\eta = 1.33$) and CDs were mixed in deionized water ($\eta = 1.33$). The absorbance was measured by a

South Korea S3100 UV–vis spectrophotometer. The PL emission intensity was measured by PL spectrometer (HORIBA Scientific FluoroMax-4) at 350 nm excitation wavelength. The quantum yield was calculated using the following equation:

$$Q = Q_R \times \frac{I}{I_R} \times \frac{A_R}{A} \times \frac{\eta^2}{\eta_R^2}$$

where Q is the quantum yield, I is the measured integrated emission intensity, A is the absorbance intensity and η is the refractive index of the respective solvents. The subscript R refers to the reference fluorophore (quinine sulfate). In order to minimize re-absorption effects, the absorbance in the 10 mm fluorescence cuvette were kept under 0.05 at the excitation wavelength of 350 nm.

Photostability and pH stability of CDs solution

The CDs solution was exposed under a 300 W xenon (Xe) lamp (Ceaulight, CEL-HXF300) for various time spans to investigate their photostability. HCl (0.1 M) or NaOH (0.1 M) was used to adjust the pH of the aqueous solution of resultant CDs.

Procedure for $Cu^{2+}$ detection

Typically, 3 mL CDs solution (0.01 mg/mL) and 1 mL $Cu^{2+}$ solution with different concentrations (20–2000 μM) were mixed and shaken at room temperature for 5 min. The fluorescence quenching spectra were immediately recorded at an excitation wavelength of 360 nm. To evaluate the detection selectivity, various metal ions such as $K^+$, $Al^{3+}$, $Mg^{2+}$, $Ca^{2+}$, $Cr^{3+}$, $Fe^{2+}$, $Fe^{3+}$, $Co^{2+}$, $Ni^{2+}$, $Cu^{2+}$, $Zn^{2+}$, and $Ba^{2+}$ were individually added into CDs solutions.

## Results and discussion

### Synthesis of CDs

As shown in Fig. 1, the various biomass including hemicelluloses, lignin, cellulose and chitosan were hydrothermally treated for producing a small amount of CDs in supernatant and more HTCs. Then, the green fluorescent CDs were prepared from biomass-HTCs

via a mild treatment of $NaOH/O_2$ solution in this experiment. In the process of hydrothermal treatment, the biopolymers are hydrolyzed and dehydrated into various small molecules including furfural aldehydes, ketones, and formic acid. The subsequent polymerization and condensation among these compounds produce the black solid product (HTC, Fig. 1) (De and Karak 2013; Sevilla and Fuertes 2009). Firstly, we used hemicelluloses as a biomass precursor to optimize the synthesis process. The SEM image in Fig. 2a shows that the HTC from hemicelluloses is composed of spherical particles with a narrow size distribution (∼ 1.2 um). Then, the resultant HTC was quickly disintegrated into CDs with intensive fluorescence emission by $NaOH/O_2$ solution treatment for 0.5–1.0 h. The conversion rate of CDs from the HTC is ultrahigh, ca. 73.5% ($CDs_{160}$, 160 °C, 1.0 h) based on the weight of HTC. Therefore, $NaOH/O_2$ treatment of HTC is a highly effective strategy to obtain CDs.

The typical TEM images (Fig. 2b, c) show that the $CDs_{160}$ is uniform with a narrow size distribution of 1.6–4.1 nm in diameter (average diameter of 2.9 nm, Fig. 2d). HR-TEM (Fig. 2c) reveals clear lattice fringes of CDs with a spacing of 0.21 nm, which can be attributed to the (100) diffraction planes of graphite (Zhang et al. 2012a). The XRD patterns shown in Fig. 2e demonstrate the graphic carbon of $CDs_{160}$ with wide peak centered at $2\theta = 24.9°$, while a broad peak at $2\theta = 21.5°$ is corresponding to the (002) peak in the patterns of HTC, indicating a high content of amorphous structure. The shifting peak correlates with the crystal transition from amorphous carbon to graphic carbon. However, the G band and D band representing graphic and amorphous carbon in Raman spectra is weak (Fig. S1, EMS) due to the fluorescent interference of CDs.

The FT-IR of $CDs_{160}$ and HTC are showed in Fig. 2f. The strong band at 3437 $cm^{-1}$ indicates the presence of –OH groups. The peaks at 2927 and 1384 $cm^{-1}$ are attributed to the stretching and bending vibrations of C–H. The strong peaks at 1590 and 1450 $cm^{-1}$ are ascribed to the stretching vibration of aromatic C=C. The peaks at 870 and 762 $cm^{-1}$ are related to the in-plane and out-plane deformations of aromatic C–H (Wang et al. 2011). Therefore, the CDs and HTC contain aromatic skeletons, revealing that aromatization takes places in hydrothermal carbonization. The aromatic structure is also a typical unit exists in lignin from pulp fibers. $NaOH/O_2$ mixture is usually

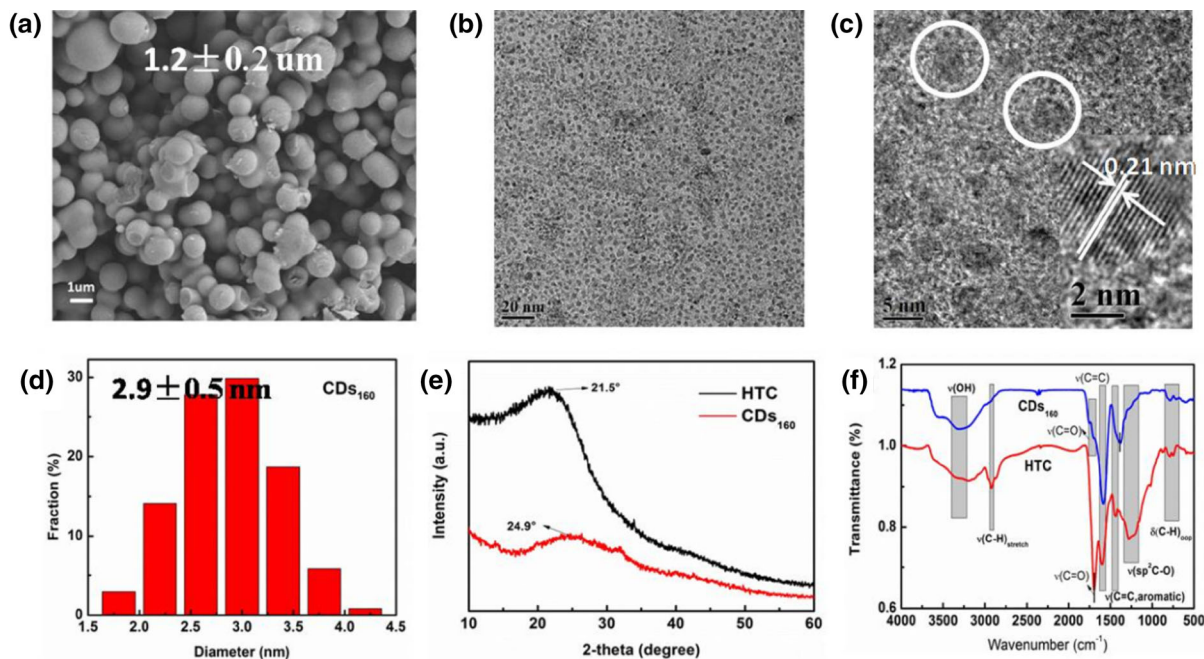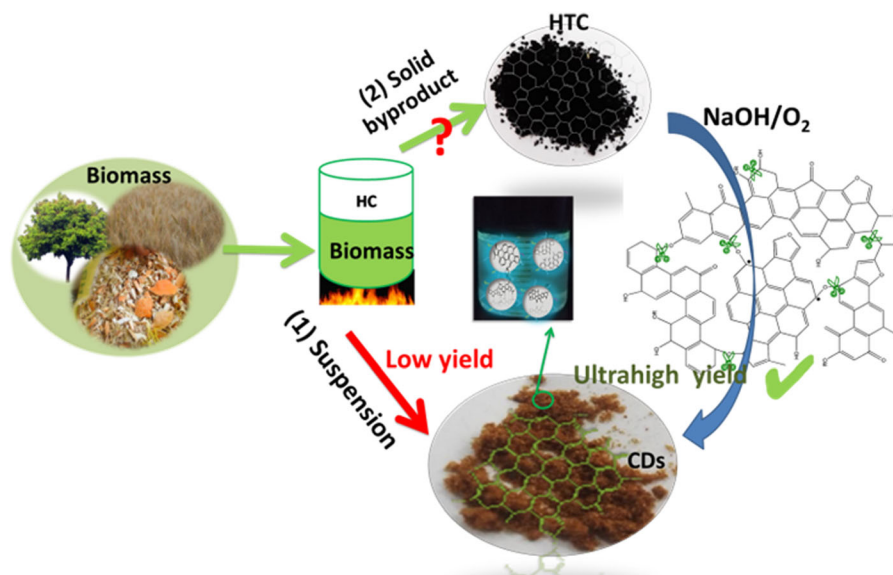**Fig. 1** High-yield synthesis of CDs from biomass hydrothermal carbon





**Fig. 2** **a** SEM image of HTC derived from hemicelluloses. **b** TEM image, **c** HR-TEM image, and **d** particle size distribution of CDs$_{160}$. **e** XRD and **f** FT-IR of CDs$_{160}$ and HTC derived from hemicelluloses

used in pulp bleaching for decomposing and removing lignin. Here, NaOH/O$_2$ solution is used to decompose HTC into pieces and finally obtained CDs. The CDs$_{160}$ shows no peak at 1261 cm$^{-1}$ (C–O–C) but a new peak at 1760 cm$^{-1}$ (C=O), indicating the ether linkage is broken and more oxygen-containing functional groups (carboxyl, ester, or carbonyl) are formed during the NaOH/O$_2$ treatment of HTC. The apparent reduce of peak at 2927 cm$^{-1}$ also shows the decrease of alkyl group in side chain after the oxidation. The elemental analysis (Table 1) demonstrates a significant decrease in carbon content from 72.7 to 37.4% and an increase in oxygen content from 21.9 to 58.6%, when the HTC was converted to CDs$_{160}$.

**Table 1** Element, size, yield, and QY of CDs$_{100-180}$ and HTC

| Sample | C(%) | H(%) | O (calculated, %) | Yield[a] (%) | Yield[b] (%) | QY (%) |
|---|---|---|---|---|---|---|
| HTC | 72.7 | 5.4 | 21.9 | 30.9 | – | – |
| CDs$_{100}$ | 42.9 | 4.2 | 52.9 | 29.1 | 94.4 | 2.8 |
| CDs$_{120}$ | 40.8 | 4.4 | 54.8 | 26.2 | 85.1 | 5.7 |
| CDs$_{140}$ | 39.5 | 4.4 | 55.1 | 23.8 | 77.0 | 9.5 |
| CDs$_{160}$ | 37.4 | 4.0 | 58.6 | 22.7 | 73.6 | 16.6 |
| CDs$_{180}$ | 35.0 | 3.8 | 61.2 | 19.6 | 63.6 | 16.6 |

[a]The yield bases on the weight of hemicelluloses

[b]The yield bases on the weight of HTC

The XPS survey spectra of HTC and CDs (Fig. 3a and 3d) show two typical peaks at 284.7 eV for C 1s and 531.4 eV for O 1s. The C/O atomic ratios of HTC and CDs160 are 1.53 and 0.62, respectively (Table S1, EMS). Thus, the elemental and XPS analysis again confirm the cleavage of ether bonds and oxidation of hydroxyl. The de-convolved high-resolution C1s spectra (Fig. 3b, e) show three C-types including C–C/C=C (284.8 eV), C–O (286.5 eV), and C=O (288.3 eV) (Qian et al. 2014). As shown in Table S1 (EMS), the atomic percentage of C–O for CDs$_{160}$ (8.88%) is lower than that of HTC (13.18%), indicating that ether cleavage occurs during the treatment of NaOH/O$_2$. And the high atomic percentage of C=O for CDs$_{160}$ (18.86%) indicates that the oxygen functional groups like aldehyde, ketone, ether

and carboxyl are formed. In the O1s spectra (Fig. 3c, f), two peaks at 531.5 eV and 533.0 eV are attributed to C=O and C–O groups respectively (Liu et al. 2017). These results also indicate that the ether linkages and hydroxyls are partially oxidized by NaOH/O$_2$ and then produce oxygen-containing groups.

In order to clarify the formation mechanism of CDs in the hydrothermal process of NaOH/O$_2$, the evolution of carbon chemical environment was further studied by $^{13}$C CP MAS NMR (Fig. 4). The peaks in 10–50, 127–160, and 170–210 ppm are attributed to $sp^3$ C–H, $sp^2$ carbon resonate of aromatic carbon, and carbonyl carbon, respectively (Baccile et al. 2009; Falco et al. 2011). The distinct peak at 128 ppm is assigned to carbon atoms in aromatic rings, indicating the existence of aromatic structure in both HTC and
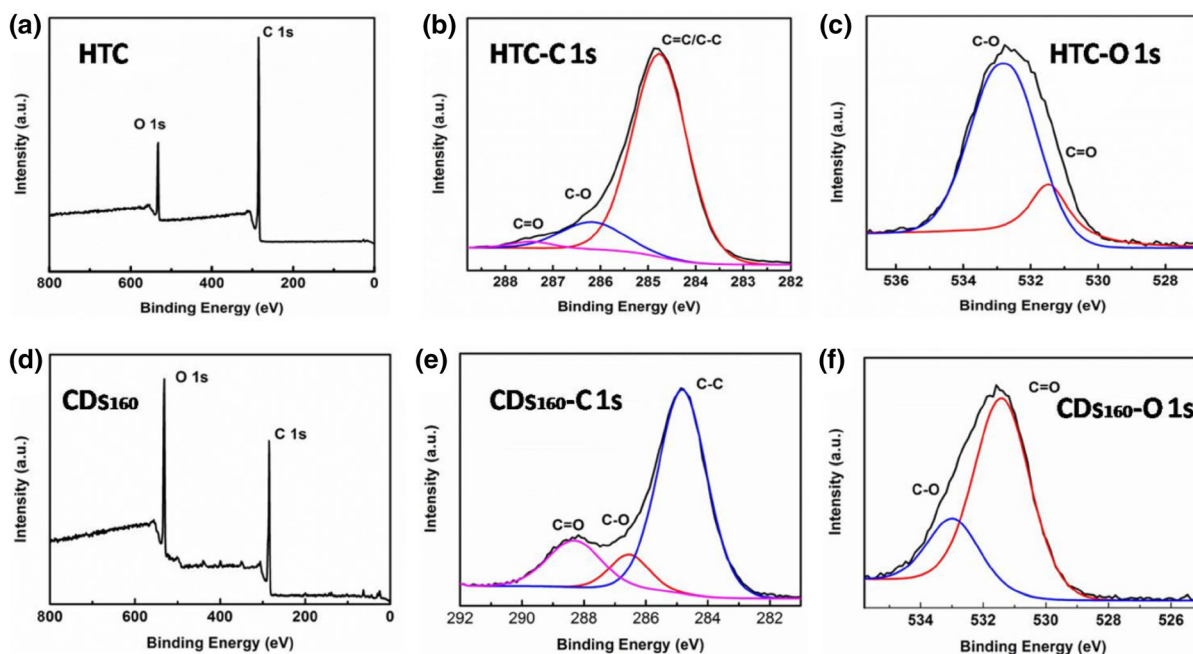


**Fig. 3** **a** XPS survey spectrum of HTC. High-resolution XPS spectra of **b** C 1s, **c** O 1s of HTC. **d** XPS survey spectrum of CDs$_{160}$. High-resolution XPS spectra of **e** C 1s and **f** O 1s of CDs$_{160}$
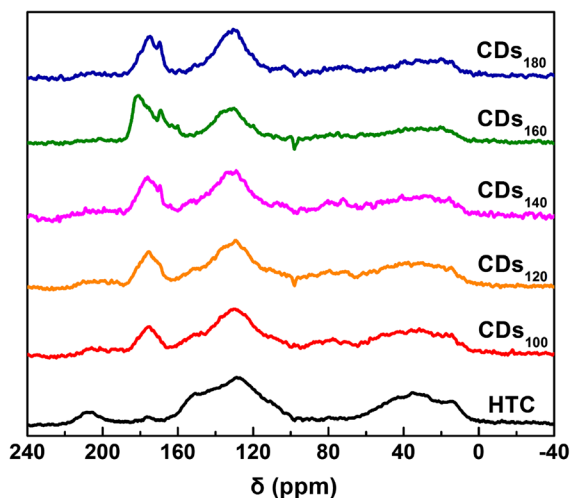
**Fig. 4** $^{13}$C CP MAS NMR spectra of HTC, CDs$_{100}$, CDs$_{120}$, CDs$_{140}$, CDs$_{160}$, and CDs$_{180}$

CDs (Titirici et al. 2008). After NaOH/O$_2$ treatment, peaks at 158 ppm (O–C=CH) and 208 ppm (C=O group in ketones and aldehydes) decline apparently, while the intensity of peak at 175 ppm (C=O group in carboxylic acid) in the oxidized products (CDs) show a significant increase of (Baccile et al. 2009; Falco et al. 2011). In addition, FT-IR and XPS demonstrate the broken of ether linkage. Therefore, the unsaturated C=O and the C–O linked with unsaturated C=C are attacked during the NaOH/O$_2$ treatment.

With molecular oxygen as an oxidant and sodium hydroxide as an active agent, the phenolic lignin containing side chain or ring conjugated carbonyl structure is effectively oxidized through nucleophilic or electrophilic reaction on the unsaturated carbonyl or carbanions. As shown in Fig. 2f, the peak at 1230 cm$^{-1}$ attributed to C–O in phenol is tiny visible. Therefore, the phenolic structure containing side chain (linked by ether bond) or ring conjugated carbonyl structure in HTC can be oxidized in NaOH/O$_2$ treatment. Then the HTC is decomposed into small pieces (i.e. CDs) with carboxylic acid on the surface. Moreover, the decrease intensity of peaks in region of 10–50 ppm (C–H) reveals the break of side chain, which is also found in FT-IR analysis.

Luminescence properties of CDs

The as-synthesized CDs$_{160}$ dispersion exhibits bright blue-green fluorescence under irradiation with 365 nm

UV light (Fig. 5a). In addition, the absorption spectra of CDs$_{160}$ show broad absorption bands at 218 nm and 261 nm. Combining results from XRD (graphic carbon), FT-IR (rich C=C), and XPS (rich C=O groups), the absorption bands can be attributed to the E-band and B-band of the π–π* transition of the well-defined conjugate aromatic structures in the carbon core, respectively (Liu et al. 2017). The result indicates that CDs$_{160}$ has electronic states with a well-defined conjugate aromatic structure, giving rise to the large energy band (Thiyagarajan et al. 2016).

Furthermore, CDs$_{160}$ shows a typical excitation-dependent fluorescence property (Fig. 5b). The emission peak gradually red-shifts from 443 to 489 nm when the excitation wavelength increases from 320 to 400 nm. The maximum emission wavelength locates at 460 nm under the excitation of 360 nm. The excitation-dependent behavior is usually attributed to the size distribution and surface chemistry, or different emissive traps (salvation effect) (Zhu et al. 2015). Due to uniform size of CDs$_{160}$, the excitation-dependent behavior of CDs$_{160}$ may result from the defects produced by the oxygen functional groups on the surface. CDs$_{160}$ also shows emission-dependent PL behavior, which means that the excitation peak gradually red-shifts from 342 to 379 nm when the emission wavelength increases from 400 to 500 nm with an increment of 20 nm (Fig. 5c). The strongest PL excitation peak appears at 360 nm under 460 nm emission, which is consistent with the PL emission spectrum with a strong emission peak at 460 nm (Fig. 5b). Furthermore, CDs$_{160}$ exhibits obvious up-conversion emission (anti-Stokes type emission) under the wavelength from 760 to 940 nm, as shown in Fig. 5d. The up-conversion PL behavior can be attributed to the simultaneous absorption of two or more photons (multi-photon activation process).

The stability of luminescent nanomaterials is an important factor to assess their applications. It is found that the fluorescence intensity of CDs$_{160}$ only slightly decreases to 97.7% of its initial intensity after 11 h irradiation, indicating that CDs$_{160}$ has excellent photo stability (Fig. 5e). Furthermore, the pH-stability was also investigated in a wide range of pH values (Fig. 5f). CDs$_{160}$ exhibits a pH-dependent PL behavior. The intensity of blue-green emission only slightly decreases at high and low pH values, but stays steady in pH ranging from 3 to 9. The effect of pH on the emission stability of CDs$_{160}$ is contributed to the
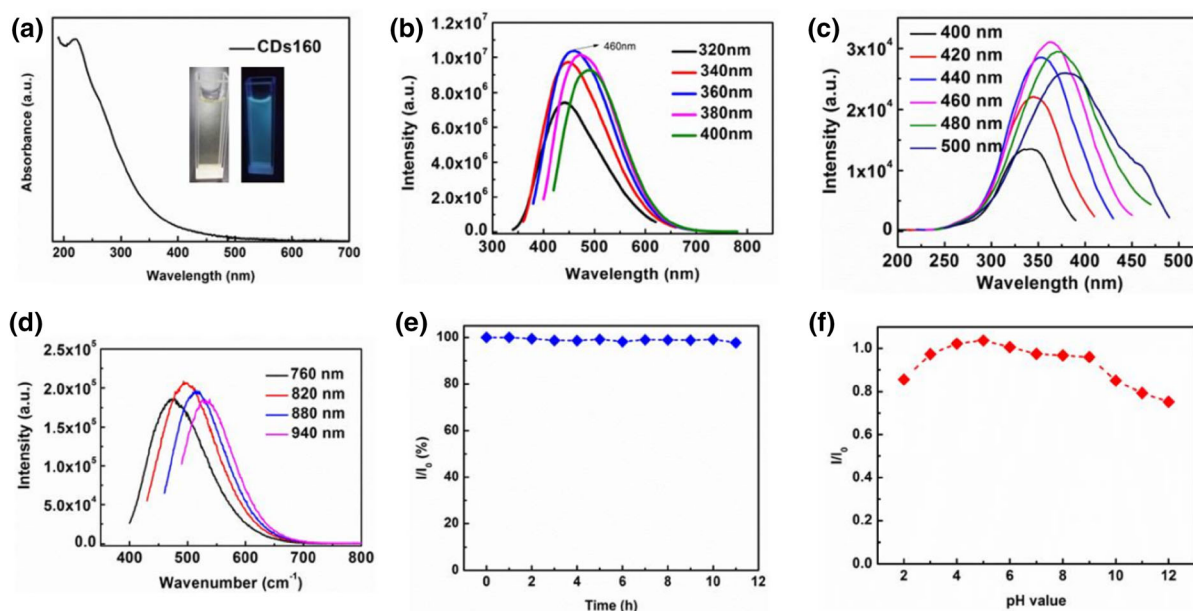
Fig. 5 a UV–vis absorption of $CDs_{160}$. Inset: the photograph of the $CDs_{160}$ suspension under sunlight (left) and UV light of 365 nm (right). b PL emission spectra excited by various incident lights progressively from 320 to 400 nm with an increment of 20 nm. c PL excitation spectra excited by various incident lights progressively from 400 to 500 nm with an increment of 20 nm. d Up-conversion PL emission spectra of $CDs_{160}$ excited by various incident lights progressively from 760 to 940 nm with an increment of 60 nm. e Photostability test of the $CDs_{160}$ suspension under continuous irradiation with Xe light. f pH-dependent PL at pH = 2–12 for $CDs_{160}$

protonation/deprotonation of carboxyl groups, which is also observed for other carboxyl-containing CDs (Ding et al. 2016; Wang et al. 2014b).

## The effect of decomposition temperature on the yield and fluorescence of CDs

In order to investigate the effect of synthesis conditions on the yield and fluorescence of CDs, the reaction time, temperature, and sodium hydroxide concentration were optimized (hemicelluloses derived HTC as a representative). As shown in Table 1, reaction time and sodium hydroxide concentration have little effect on the yield and fluorescence of CDs. On the contrary, reaction temperature plays an important role in synthesizing CDs. The yield of CDs is high up to 94.4% (based on HTC) at 100 °C, and decreases to 63.6% when temperature increasing to 180 °C. The QY of CDs, however, significantly increases from 2.2 to 16.6% when temperature rises from 100 to 180 °C. The elemental content (Table 1) indicates that CDs has a higher content of oxygen and

lower content of carbon with increasing decomposing temperature.

The results of XPS survey spectra (Fig. S2 and Table S2, EMS) show that a higher temperature (180 °C, $CDs_{180}$) leads to decrease in C–C/C=C percentage but increase in C=O percentage, suggesting that C–C/C=C in CDs are partly broken at high temperature, producing more oxygen-containing groups (C=O) on the surface of CDs. Therefore, the tunable PL QY might be attributed to the surface states of CDs that are sensitive to temperature. A yield high up to 73.5% based on the weight of HTC (22.7% based on the weight of biomass) is superior to those of CDs from other methods including hydrothermal treatment (Alam et al. 2015), microwave (Huang et al. 2017), acid oxidation (Ding et al. 2018), and carbonization (Hsu et al. 2012; Wang et al. 2016b, 2017), as shown in Table 2. Furthermore, the QY of 16.6% is also higher than or comparable to those of biomass-derived CDs from other methods (Table 2).

The chemical structures of these CDs are further confirmed by the FT-IR spectra (Fig. S3, EMS). With the increase of temperature, the bending vibration of

C–H bond at 1380 cm$^{-1}$ becomes weaker, while the vibration peak of aromatic skeleton at 1440 cm$^{-1}$ is more significant, revealing the increase of conjugate carbon (–C=C–) in the carbon core. The peak at $2\theta = 23.9°$ in the XRD pattern of CDs$_{100}$ gradually moves to higher degree with higher temperature (Fig. S4, EMS), suggesting that the carbon core is more regular and compact with raising temperature. Therefore, the increasing QY of CDs with rising reaction temperature is attributed to larger unitary emission center caused by combination of oxygen-

containing groups (C=O) and conjugated carbon atoms (Hu et al. 2015).

The average sizes are 2.3 nm, 1.3 nm, 1.9 nm, and 2.4 nm for CDs$_{100}$, CDs$_{120}$, CDs$_{140}$, and CDs$_{180}$, respectively, as shown in Fig. 6a–d. The PL spectra of CDs$_{100}$, CDs$_{120}$, CDs$_{140}$, and CDs$_{180}$ all show typical excitation-dependent fluorescence property (Fig. 6e–h). The peak of PL emission does not show obvious shift when the size of the CDs changes from 1.3 to 2.4 nm (Fig. S5), indicating that the origin of blue-green emission is attributed to the special edge states formed from hybridization of the carbon backbone, the

**Table 2** Comparison of yield and QY of CDs from various synthesis methods

| Synthetic method | Material | Yield (%) | QY (%) | References |
|---|---|---|---|---|
| Hydrothermal treatment | Apple juice | – | 4.27 | Mehta et al. (2015) |
| Hydrothermal treatment | Cabbage | 7.07 | 16.5 | Alam et al. (2015) |
| Hydrothermal treatment | *Bombyx mori* silk | – | 13.9 | Wu et al. (2013) |
| Hydrothermal treatment | Sweet potato | – | 8.64 | Shen et al. (2017) |
| Hydrothermal treatment | Aloe | – | 10.37 | Xu et al. (2015) |
| Hydrothermal treatment | Plant petals | – | 6.5 | Shi et al. (2015) |
| Hydrothermal treatment | Glucose/glutathione | – | 7.2 | Wang et al. (2015) |
| Microwave treatment | Banana peels | 16 | – | Huang et al. (2017) |
| Microwave-assisted pyrolysis | Tomato/EDA and urea | – | 1.8–8.5 | Liu et al. (2017) |
| Solvothermal carbonization | Chitosan/EDA | – | 5.7–10.4 | Zhang et al. (2018) |
| Carbonization/acid oxidation/amine functionalization | Leaves | – | 1–2 | Suryawanshi et al. (2014) |
| Sulfuric acid carbonization/passivation | Carbohydrates | – | 1–13 | Peng and Travas-Sejdic (2009) |
| Nitric acid oxidation/hydrothermal treatment | Lignin | 21 | 21 | Ding et al. (2018) |
| Acid hydrolysis | a-cellulose | – | 4.0–6.4 | Ng et al. (2017) |
| Carbonization/acid oxidation | Rice husk | 10 | – | (Wang et al. 2017) |
| Carbonization/alkaline activation/acid oxidation | Rice husks | 8.1 | 2 | Wang et al. (2016b) |
| Two-step carbonization | Soybeans | – | 3.17 | Xu et al. (2016) |
| Carbonization | Coffee grounds | 12 | 3.8 | Hsu et al. (2012) |
| NaOH/O$_2$ treatment | Hemicellulose | 22.7[a] (73.5)[b] | 16.6 | This work |
| NaOH/O2 treatment | Chitosan | 33.5[a] (99.0)[b] | 11.7 | This work |
| NaOH/O2 treatment | Cellulose | 34.0[a] (90.2)[b] | 13.4 | This work |
| NaOH/O2 treatment | Lignin | 42.5[a] (67.0)[b] | 10.0 | This work |

[a] The yield bases on the weight of biomass

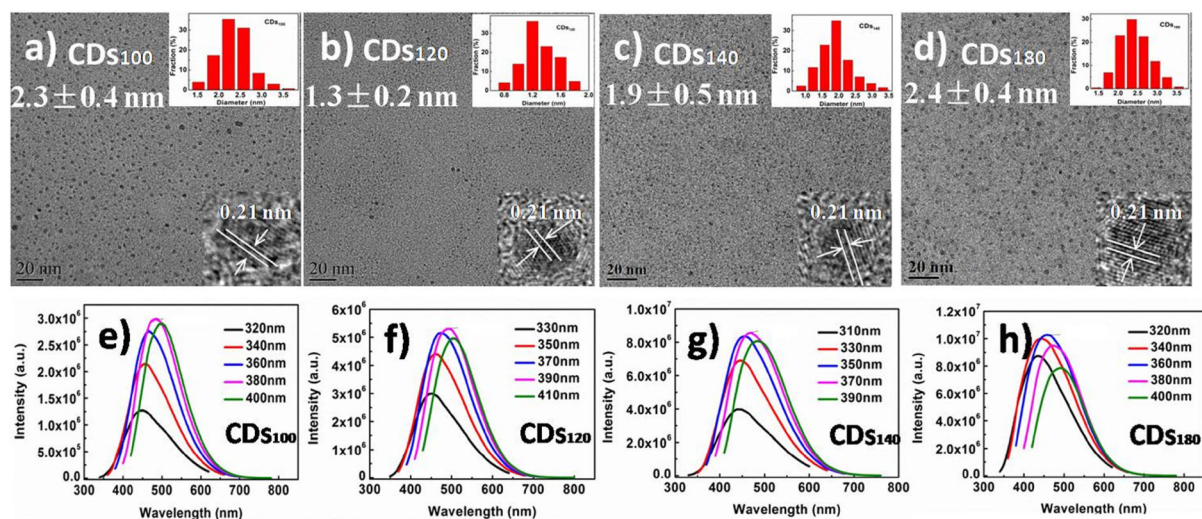[b] The yield bases on the weight of HTC

**Fig. 6** The TEM, HR-TEM images, size distributions, and PL emission spectra (excited by various incident lights progressively with an increment of 20 nm) of CDs$_{100}$ (**a**, **e**), CDs$_{120}$ (**b**, **f**), CDs$_{140}$ (**c**, **g**), and CDs$_{180}$ (**d**, **h**), respectively

carboxyl and carbonyl groups (C=O) at the edge of the CDs (Wang et al. 2014b) rather than the quantumn size effect (Li et al. 2010). A larger unitary emission center with growing temperature results in higher PL strength but no significant change in the emission peak positions of PL, due to the unaltered emission center of these CDs.

## Detection of Cu$^{2+}$

Figure 7a displays the fluorescence intensities of the CDs$_{160}$ solutions with different metal ions at 460 nm. Cu$^{2+}$ could quench the fluorescence of CDs more effectively as compared with other metal ions. The fluorescence emission spectra of CDs at different Cu$^{2+}$ concentrations are shown in Fig. 7b. Upon excitation at 360 nm, the emission intensity decreases with increasing concentration of Cu$^{2+}$. Efficient fluorescence quench at a low Cu$^{2+}$ concentration can still be observed. Moreover, no significant change in the peak wavelength or shape of the emission spectrum is found, suggesting a strong interaction between Cu$^{2+}$ and surface functionalities (hydroxyl or carboxyl groups) on the CDs (Zhang et al. 2019). The fluorescence emission intensity of CDs-Cu$^{2+}$ system decreases monotonously with an increase in the concentration of Cu$^{2+}$ within 400 μmol L$^{-1}$ (Fig. 7c). The effect of Cu$^{2+}$ on the CDs fluorescence intensity was evaluated and a linear correlation was obtained with an equation of, I$_0$/I = 1.0438 + 0.0651[Cu$^{2+}$] at

the range of 5–30 μM. The fluorescence quench can be modeled by a Stern–Volmer equation (I$_0$/I = 1 + K$_{SV}$[Cu$^{2+}$]), with K$_{SV}$ = 65100 M$^{-1}$ and r = 0.984 (the inset in Fig. 7). The detection limit for Cu$^{2+}$ was as low as 85 nM based on three times of the standard deviation rule (LOD = 3σ/k, n = 10), satisfying the sensitivity requirement of Cu$^{2+}$ detection for drinking water (20 μM) (Fitzgerald 1998). These results imply that the CDs fluorescence probe has potential application in Cu$^{2+}$ detection.

Our approach can also be applied in synthesizing CDs from various biomass resources with both high yield and QY. For example, the CDs were prepared from HTC (240 °C, 6 h) derived from lignin, cellulose, and chitosan at 160 °C for 1 h. As shown in Fig. 8, these HTCs (Fig. 8a–c) with spherical particles or schistose and fragmentary structure are decomposed to uniformly-dispersed CDs with size of about 2 nm and clear lattice fringes (Fig. 8d–f). Figure 8g–i show that the PL emission spectra of CDs is typical excitation-dependent. Fig. S6 (EMS) shows the UV–Vis absorbance of these CDs dispersions. The broad absorption bands at 200–300 nm are attributed to π–π* transition of the carbon core and n–π* transition of C=O. The QYs of CDs from lignin, cellulose, and chitosan derived carbons are 10.0%, 13.4% and 11.7%, with yields of 67.0%, 90.2%, and 99.0% based on the weight of HTC (42.5%, 34.0%, and 33.5% based on the weight of biomass, Table 2), respectively. Therefore, this approach is effective and
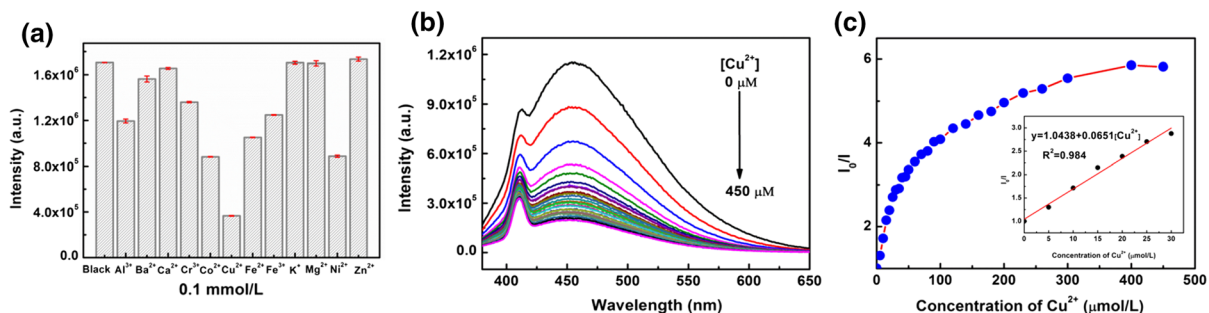
**Fig. 7** **a** The difference in PL intensity of $CDs_{160}$ dispersion between the blank and solutions containing different metal ions (excitation at 360 nm; $[M^{n+}] = 100$ μM, fluorescence intensities of $CDs_{160}$ were recorded at 460 nm in different ions). **b** PL spectra of $CDs_{160}$ dispersion in the presence of different

Cu²⁺ concentrations (from top to bottom: 0–450 μM). **c** Stern–Volmer plot for the quenching of $CDs_{160}$ PL by Cu²⁺ (excitation at 360 nm; $I_0$ and $I$ are $CDs_{160}$ fluorescence intensities at 460 nm in the absence and presence of Cu²⁺, respectively
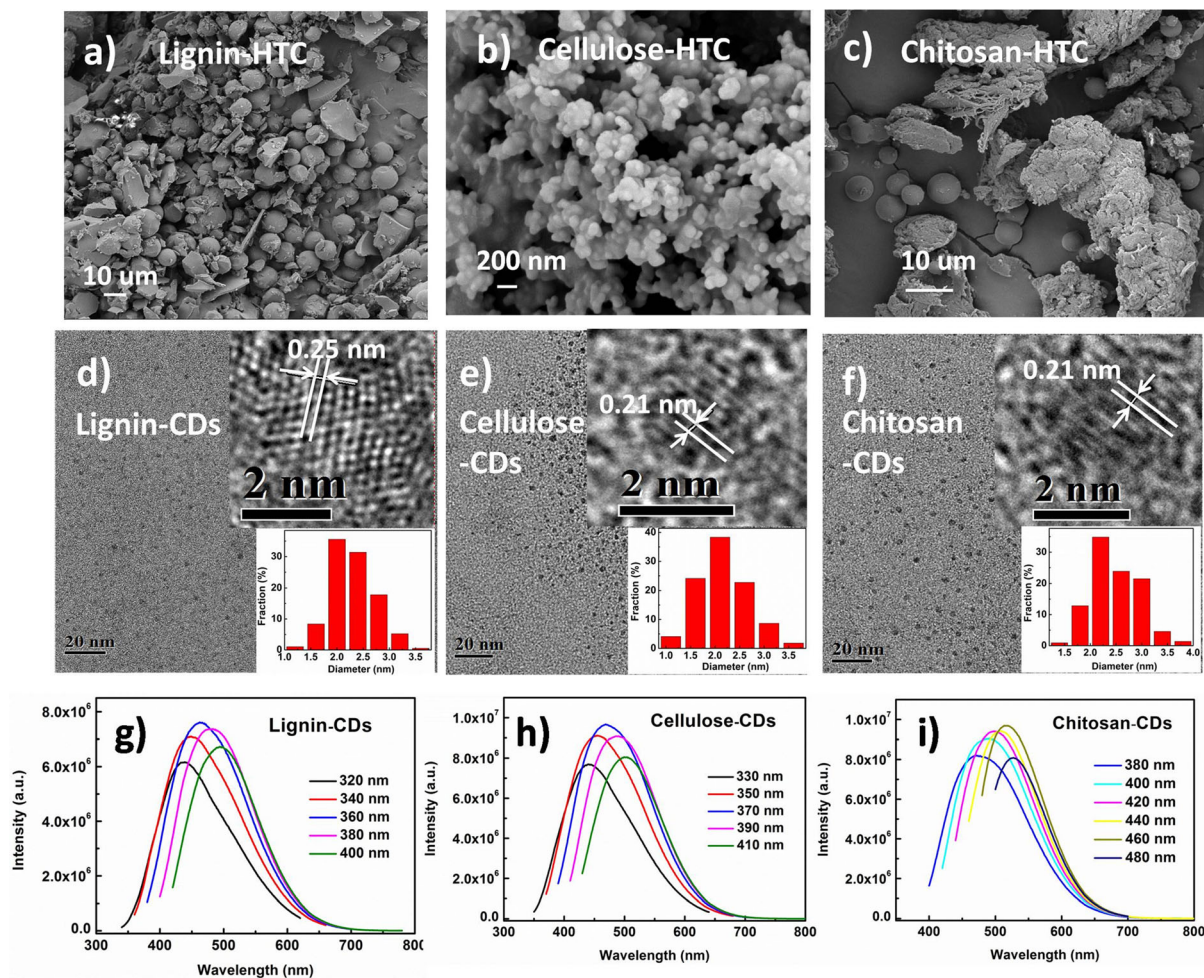


**Fig. 8** SEM images of HTCs derived from lignin (**a**), cellulose (**b**), and chitosan (**c**). TEM images and size distribution, and PL spectra (excited by various incident lights progressively with an

increment of 20 nm) of lignin-CDs (**d**, **g**), cellulose-CDs (**e**, **h**), and chitosan-CDs (**f**, **i**) obtained at 160 °C

universal for large-scaly producing CDs from various biomass resources.

## Conclusion

In summary, we develop an environment-friendly, simple, universal, and highly-effective route for high-yield production of fluorescent CDs from low-cost and renewable biomass hydrothermal carbons with low-concentration $NaOH/O_2$ solution. As compared with the current methods, our approach offers ultrahigh CDs yields for various biomass resources. The as-prepared CDs exhibit excellent optical properties, including high QY, up-conversion performance, and photostability. The QY of CDs, determined by the surface states and conjugated structure of the carbon core, can be easily tailored by changing the reaction temperature. The CDs can be used as a fluorescence probe for $Cu^{2+}$ detection with low concentration. Thus, our work provides a new way for the low-cost and green synthesis of CDs from renewable resources.

### Compliance with ethical standards

**Conflict of interest** There are no conflict of interest to declare.

## References

Alam AM, Park BY, Ghouri ZK, Park M, Kim HY (2015) Synthesis of carbon quantum dots from cabbage with down- and up-conversion photoluminescence properties: excellent imaging agent for biomedical applications. Green Chem 17:3791–3797. https://doi.org/10.1039/c5gc00686d

Baccile N, Laurent G, Babonneau F, Fayon F, Titirici M, Antonietti M (2009) Structural characterization of hydrothermal carbon spheres by advanced solid-state MAS 13C NMR investigations. J Phys Chem C 113:9644–9654. https://doi.org/10.1021/jp901582x

Bao L, Zhang ZL, Tian ZQ, Zhang L, Liu C, Lin Y, Qi B, Pang DW (2011) Electrochemical tuning of luminescent carbon nanodots: from preparation to luminescence mechanism. Adv Mater 23:5801–5806. https://doi.org/10.1002/adma.201102866

Chen W, Hu C, Yang Y, Cui J, Liu Y (2016) Rapid synthesis of carbon dots by hydrothermal treatment of lignin. Materials 9:184. https://doi.org/10.3390/ma9030184

De B, Karak N (2013) A green and facile approach for the synthesis of water soluble fluorescent carbon dots from banana Juice. RSC Adv 3:8286–8290. https://doi.org/10.1039/c3ra00088e

Ding H, Yu SB, Wei JS, Xiong HM (2016) Full-color light-emitting carbon dots with a surface-state-controlled luminescence mechanism. ACS Nano 10:484–491. https://doi.org/10.1021/acsnano.5b05406

Ding Z, Li F, Wen J, Wang X, Sun R (2018) Gram-scale synthesis of single-crystalline graphene quantum dots derived from lignin biomass. Green Chem 20(6):1383–1390. https://doi.org/10.1039/c7gc03218h

Falco C, Baccile N, Titirici MM (2011) Morphological and structural differences between glucose, cellulose and lignocellulosic biomass derived hydrothermal carbons. Green Chem 13:3273–3281. https://doi.org/10.1039/C1GC15742F

Fitzgerald DJ (1998) Safety guidelines for copper in water. Am J Clin Nutr 67:1098S–1102S. https://doi.org/10.1093/ajcn/67.5.1098S

Gao J, Zhu M, Huang H, Liu Y, Kang Z (2017) Advances, challenges and promises of carbon dots. Inorg Chem Front 4:1963–1986. https://doi.org/10.1039/c7qi00614d

He X, Li H, Liu Y, Huang H, Kang Z, Lee ST (2011) Water soluble carbon nanoparticles: hydrothermal synthesis and excellent photoluminescence properties. Colloids Surf B Biointerfaces 87:326–332. https://doi.org/10.1016/j.colsurfb.2011.05.036

Hsu PC, Shih ZY, Lee CH, Chang HT (2012) Synthesis and analytical applications of photoluminescent carbon nanodots. Green Chem 14:917–920. https://doi.org/10.1039/c2gc16451e

Hu SL, Niu KY, Sun J, Yang J, Zhao NQ, Du XW (2009) One-step synthesis of fluorescent carbon nanoparticles by laser irradiation. J Mater Chem 19:484–488. https://doi.org/10.1039/b812943f

Hu Y, Yang J, Jia L, Yu JS (2015) Ethanol in aqueous hydrogen peroxide solution: hydrothermal synthesis of highly photoluminescent carbon dots as multifunctional nanosensors. Carbon 93:999–1007. https://doi.org/10.1016/j.carbon.2015.06.018

Huang Q, Lin X, Zhu JJ, Tong QX (2017) Pd-Au@carbon dots nanocomposite: facile synthesis and application as an ultrasensitive electrochemical biosensor for determination of colitoxin DNA in human serum. Biosens Bioelectron 94:507–512. https://doi.org/10.1016/j.bios.2017.03.048

Jaiswal A, Ghosh SS, Chattopadhyay A (2012) One step synthesis of C-dots by microwave mediated caramelization of poly(ethylene glycol). Chem Commun 48:407–409. https://doi.org/10.1039/c1cc15988g

Li H, He X, Kang Z, Huang H, Liu J, Lian S, Tsang CHA, Yang X, Lee ST (2010) Water-soluble fluorescent carbon quantum dots and photocatalyst design. Angew Chem Int Ed 49:4430–4434. https://doi.org/10.1002/anie.200906154

Li H, Liu R, Lian S, Liu Y, Huang H, Kang Z (2013a) Near-infrared light controlled photocatalytic activity of carbon quantum dots for highly selective oxidation reaction.

Nanoscale 5:3289–3297. https://doi.org/10.1039/c3nr00092c

Li W, Zhang Z, Kong B, Feng S, Wang J, Wang L, Yang J, Zhang F, Wu P, Zhao D (2013b) Simple and green synthesis of nitrogen-doped photoluminescent carbonaceous nanospheres for bioimaging. Angew Chem Intl Ed 52:8151–8155. https://doi.org/10.1002/anie.201303927

Li H, Liu J, Guo S, Zhang Y, Huang H, Liu Y, Kang Z (2015) Carbon dots from PEG for highly sensitive detection of levodopa. J Mater Chem B 3:2378–2387. https://doi.org/10.1039/c4tb01983k

Liu S, Tian J, Wang L, Zhang Y, Qin X, Luo Y, Asiri AM, Al-Youbi AO, Sun X (2012) Hydrothermal treatment of grass: a low-cost, green route to nitrogen-doped, carbon-rich, photoluminescent polymer nanodots as an effective fluorescent sensing platform for label-free detection of Cu(II) ions. Adv Mater 24:2037–2041. https://doi.org/10.1002/adma.201200164

Liu W, Li C, Sun X, Pan W, Yu G, Wang J (2017) Highly crystalline carbon dots from fresh tomato: UV emission and quantum confinement. Nanotechnology 28:485705. https://doi.org/10.1088/1361-6528/aa900b

Liu J, Li D, Zhang K, Yang M, Sun H, Yang B (2018a) One-step hydrothermal synthesis of nitrogen-doped conjugated carbonized polymer dots with 31% efficient red emission for in vivo imaging. Small 14:1703919. https://doi.org/10.1002/smll.201703919

Liu W, Xu S, Guan S, Liang R, Wei M, Evans DG, Duan X (2018b) Confined synthesis of carbon nitride in a layered host matrix with unprecedented solid-state quantum yield and stability. Adv Mater 30:1704376. https://doi.org/10.1002/adma.201704376

Mehta VN, Jha S, Basu H, Singhal RK, Kailasa SK (2015) One-step hydrothermal approach to fabricate carbon dots from apple juice for imaging of mycobacterium and fungal cells. Sens Actuators B Chem 213:434–443. https://doi.org/10.1016/j.snb.2015.02.104

Ng YH, Chin SF, Pang SC, Ng SM (2017) The luminescence profile of carbon dots synthesized from α-cellulose under different acid hydrolysis conditions. Opt Mater 70:50–56. https://doi.org/10.1016/j.optmat.2017.05.014

Peng H, Travas-Sejdic J (2009) Simple aqueous solution route to luminescent carbogenic dots from carbohydrates. Chem Mater 21:5563–5565. https://doi.org/10.1021/cm901593y

Qian Z, Ma J, Shan X, Feng H, Shao L, Chen J (2014) Highly luminescent N-doped carbon quantum dots as an effective multifunctional fluorescence sensing platform. Chem Eur J 20:2254–2263. https://doi.org/10.1002/chem.201304374

Qin X, Lu W, Asiri AM, Al-Youbi AO, Sun X (2013) Green, low-cost synthesis of photoluminescent carbon dots by hydrothermal treatment of willow bark and their application as an effective photocatalyst for fabricating Au nanoparticles–reduced graphene oxide nanocomposites for glucose detection. Catal Sci Technol 3:1027–1035. https://doi.org/10.1039/c2cy20635h

Ran X, Sun H, Pu F, Ren J, Qu X (2013) Ag nanoparticle-decorated graphene quantum dots for label-free, rapid and sensitive detection of Ag+ and biothiols. Chem Commun 49:1079–1081. https://doi.org/10.1039/c2cc38403e

Sevilla M, Fuertes AB (2009) The production of carbon materials by hydrothermal carbonization of cellulose. Carbon 47:2281–2289. https://doi.org/10.1016/j.carbon.2009.04.026

Shen J, Shang S, Chen X, Wang D, Cai Y (2017) Facile synthesis of fluorescence carbon dots from sweet potato for $Fe^{3+}$ sensing and cell imaging. Mater Sci Eng C Mater Biol Appl 76:856–864. https://doi.org/10.1016/j.msec.2017.03.178

Shi L, Li Y, Li X, Wen X, Zhang G, Yang J, Dong C, Shuang S (2015) Facile and eco-friendly synthesis of green fluorescent carbon nanodots for applications in bioimaging, patterning and staining. Nanoscale 7:7394–7401. https://doi.org/10.1039/c5nr00783f

Suryawanshi A, Biswal M, Mhamane D, Gokhale R, Patil S, Guin D, Ogale S (2014) Large scale synthesis of graphene quantum dots (GQDs) from waste biomass and their use as an efficient and selective photoluminescence on-off-on probe for Ag+ ions. Nanoscale 6:11664–11670. https://doi.org/10.1039/c4nr02494j

Thiyagarajan SK, Raghupathy S, Palanivel D, Raji K, Ramamurthy P (2016) Fluorescent carbon nano dots from lignite: unveiling the impeccable evidence for quantum confinement. Phys Chem Chem Phys 18:12065–12073. https://doi.org/10.1039/c6cp00867d

Titirici MM, Antonietti M, Baccile N (2008) Hydrothermal carbon from biomass: a comparison of the local structure from poly-to monosaccharides and pentoses/hexoses. Green Chem 10:1204–1212. https://doi.org/10.1039/B807009A

Wang Y, Hu A (2014) Carbon quantum dots: synthesis, properties and applications. J Mater Chem C 2:6921–6939. https://doi.org/10.1039/c4tc00988f

Wang X, Qu K, Xu B, Ren J, Qu X (2011) Microwave assisted one-step green synthesis of cell-permeable multicolor photoluminescent carbon dots without surface passivation reagents. J Mater Chem 21:2445–2450. https://doi.org/10.1039/c0jm02963g

Wang L, Wang Y, Xu T, Liao H, Yao C, Liu Y, Li Z, Chen Z, Pan D, Sun L, Wu M (2014a) Gram-scale synthesis of single-crystalline graphene quantum dots with superior optical properties. Nat Commun 5:5357. https://doi.org/10.1038/ncomms6357

Wang L, Zhu SJ, Wang HY, Qu SN, Zhang YL, Zhang JH, Chen QD, Xu HL, Han W, Yang B, Sun HB (2014b) Common origin of green luminescence in carbon nanodots and graphene quantum dots. ACS Nano 8:2541–2547. https://doi.org/10.1021/nn500368m

Wang C, Xu Z, Cheng H, Lin H, Humphrey MG, Zhang C (2015) A hydrothermal route to water-stable luminescent carbon dots as nanosensors for pH and temperature. Carbon 82:87–95. https://doi.org/10.1016/j.carbon.2014.10.035

Wang L, Li B, Xu F, Shi X, Feng D, Wei D, Li Y, Feng Y, Wang Y, Jia D, Zhou Y (2016a) High-yield synthesis of strong photoluminescent N-doped carbon nanodots derived from hydrosoluble chitosan for mercury ion sensing via smartphone APP. Biosens Bioelectron 79:1–8. https://doi.org/10.1016/j.bios.2015.11.085

Wang Z, Yu J, Zhang X, Li N, Liu B, Li Y, Wang Y, Wang W, Li Y, Zhang L, Dissanayake S, Suib SL, Sun L (2016b) Large-scale and controllable synthesis of graphene quantum dots from rice husk biomass: a comprehensive utilization

strategy. ACS Appl Mater Interfaces 8:1434–1439. https://doi.org/10.1021/acsami.5b10660

Wang Z, Liu J, Wang W, Wei Z, Wang F, Gong P, Wang J, Li N, Liu B, Zhang Z, Wang W, Sun L (2017) Photoluminescent carbon quantum dot grafted silica nanoparticles directly synthesized from rice husk biomass. J Mater Chem B 5:4679–4689. https://doi.org/10.1039/c7tb00811b

Wei J, Shen J, Zhang X, Guo S, Pan J, Hou X, Zhang H, Wang L, Feng B (2013) Simple one-step synthesis of water-soluble fluorescent carbon dots derived from paper ash. RSC Adv 3:13119–13122. https://doi.org/10.1039/c3ra41751d

Wu ZL, Zhang P, Gao MX, Liu CF, Wang W, Leng F, Huang CZ (2013) One-pot hydrothermal synthesis of highly luminescent nitrogen-doped amphoteric carbon dots for bioimaging from *Bombyx mori* silk—natural proteins. J Mater Chem B 1:2868–2873. https://doi.org/10.1039/c3tb20418a

Xiong Y, Schneider J, Reckmeier CJ, Huang H, Kasak P, Rogach AL (2017) Carbonization conditions influence the emission characteristics and the stability against photobleaching of nitrogen doped carbon dots. Nanoscale 9:11730–11738. https://doi.org/10.1039/c7nr03648e

Xu H, Yang X, Li G, Zhao C, Liao X (2015) Green synthesis of fluorescent carbon dots for selective detection of tartrazine in food samples. J Agric Food Chem 63:6707–6714. https://doi.org/10.1021/acs.jafc.5b02319

Xu M, Huang Q, Sun R, Wang X (2016) Simultaneously obtaining fluorescent carbon dots and porous active carbon for supercapacitors from biomass. RSC Adv 6:88674–88682. https://doi.org/10.1039/c6ra18725k

Yang Y, Cui J, Zheng M, Hu C, Tan S, Xiao Y, Yang Q, Liu Y (2012) One-step synthesis of amino-functionalized fluorescent carbon nanoparticles by hydrothermal carbonization of chitosan. Chem Commun 48:380–382. https://doi.org/10.1039/c1cc15678k

Yang G, Wan X, Su Y, Zeng X, Tang J (2016) Acidophilic S-doped carbon quantum dots derived from cellulose fibers and their fluorescence sensing performance for metal ions in an extremely strong acid environment. J Mater Chem A 4:12841–12849. https://doi.org/10.1039/c6ta05943k

Ye R, Xiang C, Lin J, Peng Z, Huang K, Yan Z, Cook NP, Samuel ELG, Huang CC, Ruan G, Ceriotti G, Raji ARO, Martí AA, Tour JM (2013) Coal as an abundant source of graphene quantum dots. Nat Commun 4:2943. https://doi.org/10.1038/ncomms3943

Yuan M, Zhong R, Gao H, Li W, Yun X, Liu J, Zhao X, Zhao G, Zhang F (2015) One-step, green, and economic synthesis of water-soluble photoluminescent carbon dots by hydrothermal treatment of wheat straw, and their bio-applications in labeling, imaging, and sensing. Appl Surf Sci 355:1136–1144. https://doi.org/10.1016/j.apsusc.2015.07.095

Yuan F, Wang Z, Li X, Li Y, Tan Z, Fan L, Yang S (2017) Bright multicolor bandgap fluorescent carbon quantum dots for electroluminescent light-emitting diodes. Adv Mater 29:1604436. https://doi.org/10.1002/adma.201604436

Yuan JM, Zhao R, Wu ZJ, Li W, Yang XG (2018) Graphene oxide quantum dots exfoliated from carbon fibers by microwave irradiation: two photoluminescence centers and self-assembly behavior. Small 14:1703714. https://doi.org/10.1002/smll.201703714

Zhang YQ, Ma DK, Zhuang Y, Zhang X, Chen W, Hong LL, Yan QX, Yu K, Huang SM (2012a) One-pot synthesis of N-doped carbon dots with tunable luminescence properties. J Mater Chem 22:16714–16718. https://doi.org/10.1039/c2jm32973e

Zhang Z, Hao J, Zhang J, Zhang B, Tang J (2012b) Protein as the source for synthesizing fluorescent carbon dots by a one-pot hydrothermal route. RSC Adv 2:8599. https://doi.org/10.1039/c2ra21217j

Zhang DW, Papaioannou N, David NM, Luo H, Gao H, Tanase LC, Degousée T, Samori P, Sapelkin A, Fenwick O, Titirici MM, Krause S (2018) Photoelectrochemical response of carbon dots (CDs) derived from chitosan and their use in electrochemical imaging. Mater Horiz 5:423–428. https://doi.org/10.1039/c7mh00784a

Zhang Y, Gao Z, Yang X, Chang J, Liu Z, Jiang K (2019) Fish-scale-derived carbon dots as efficient fluorescent nanoprobes for detection of ferric ions. RSC Adv 9:940–949. https://doi.org/10.1039/c8ra09471c

Zhao QL, Zhang ZL, Huang BH, Peng J, Zhang M, Pang DW (2008) Facile preparation of low cytotoxicity fluorescent carbon nanocrystals by electrooxidation of graphite. Chem Commun 41:5116–5118. https://doi.org/10.1039/b812420e

Zhu S, Meng Q, Wang L, Zhang J, Song Y, Jin H, Zhang K, Sun H, Wang H, Yang B (2013) Highly photoluminescent carbon dots for multicolor patterning, sensors, and bioimaging. Angew Chem Int Ed 52:3953–3957. https://doi.org/10.1002/anie.201300519

Zhu Y, Wu Z, Jing M, Hou H, Yang Y, Zhang Y, Yang X, Song W, Jia X, Ji X (2015) Porous $NiCo_2O_4$ spheres tuned through carbon quantum dots utilised as advanced materials for an asymmetric supercapacitor. J Mater Chem A 3:866–877. https://doi.org/10.1039/c4ta05507a